2006 IEEE Conference on
Systems, Man, and Cybernetics
October 8-11, 2006, Taipei, Taiwan

Special Session: "Security and Assurance in Information and Multimedia Systems (S16)"

Predictive-Transform Source Coding With Subbands

Erlan H. Feria

***Abstract* --- Minimum mean squared error (MMSE) predictive-transform (PT) source coding is integrated with subband compression to further improve the performance of low bit rate MMSE PT source coders. A desirable byproduct of the advanced scheme is that the incorporation of joint optimum prediction and transformation from subband to subband is ideally suited to its integration with JPEG2000 to yield even higher compression levels while producing an outstanding objective as well as subjective visual performance.**

I. Introduction

Recently it was shown that wavelets based JPEG2000 [1] can yield remarkably 'poor' results when applied to synthetic aperture radar (SAR) images [2] that are being used in knowledge-aided airborne moving target indicator (AMTI) radar applications [5]. To demonstrate these surprising results a very simple strip-processor minimum mean squared error (MMSE) predictive-transform (PT) source coder was used [2]. The reason for JPEG2000's poor performance, more than 5 dBs worse for the SAR image under test [5], may be traced to the significant difference in correlation between adjacent horizontal and adjacent vertical pixels found in typical SAR images. Fortunately PT source coding offers a very simple solution to this problem. This is the case since its optimum design of prediction and transformation matrices in a flexible pixel geometry processing environment explicitly takes into consideration the vastly different horizontal and vertical pixel correlations. In addition, there are now available fast on-line PT implementation algorithms that are based on even/odd eigenvector decompositions [4] and/or Hadamard structures [6]. However, for standard images such as those given in the JPEG suitcase as well as the Lena image it has been found that JPEG2000 performs satisfactorily. This is due to the use of subband coding that produces an exceptionally appealing objective and subjective visual performance when the correlation between adjacent horizontal and adjacent vertical pixels does not vary significantly, as is the case for this type of images. On the other hand, the current predictive-transform strategy still needs to be refined to yield results that are significantly superior to those of JPEG2000 when compressing images such as those found in the JPEG suitcase. However, since JPEG2000 does not use prediction from subband to subband it stands to reason that the structural flexibility of MMSE PT source coding may be transported to subband coding to achieve even better results. This is the problem that is addressed in this paper for which very promising preliminary results are advanced.

The rest of this manuscript is presented in two sections. In Section II the pre-requisite PT source coding background material is given and in Section III the proposed integration of MMSE PT source coding with subband compression is advanced along with future research ideas.

E. H. Feria is with the Department of Engineering Science and Physics at the College of Staten Island of the City University of New York, 2800 Victory Blvd., Staten Island, NY 10314, USA, feria@mail.csi.cuny.edu

II. Background

In Fig. 1 the overall PT source coder architecture is shown. It has as its input the output of a signal source **y**. As an illustration this output will be assumed to be a real matrix representing 2-D images. The structure consists of two distinct sections. In the upper section the lossy encoder and associated lossy decoder are depicted while in the lower section the lossless encoder and decoder are shown. The lossless section of the coder is explained in detail in [2] and will not be discussed here since it is generally different from that used in subband compression [1]. In Fig. 2 the lossy PT encoder structure is shown. It consists of a transform pre-processor $f_T(\mathbf{y})$ whose output $\mathbf{x}_k$ is a real n dimensional column vector. In Fig. 3 an image illustration is given where **y** is a matrix consisting of 64 real valued picture elements or pixels and the transform pre-processor produces sixteen n=4 dimensional pixel vectors $\{\mathbf{x}_k\text{:k=1,…,16}\}$. The pixel vector

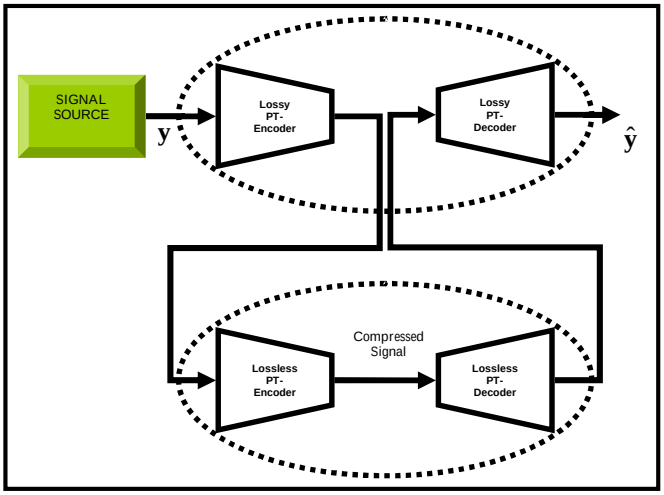

Fig. 1 The PT Source Coder Architecture

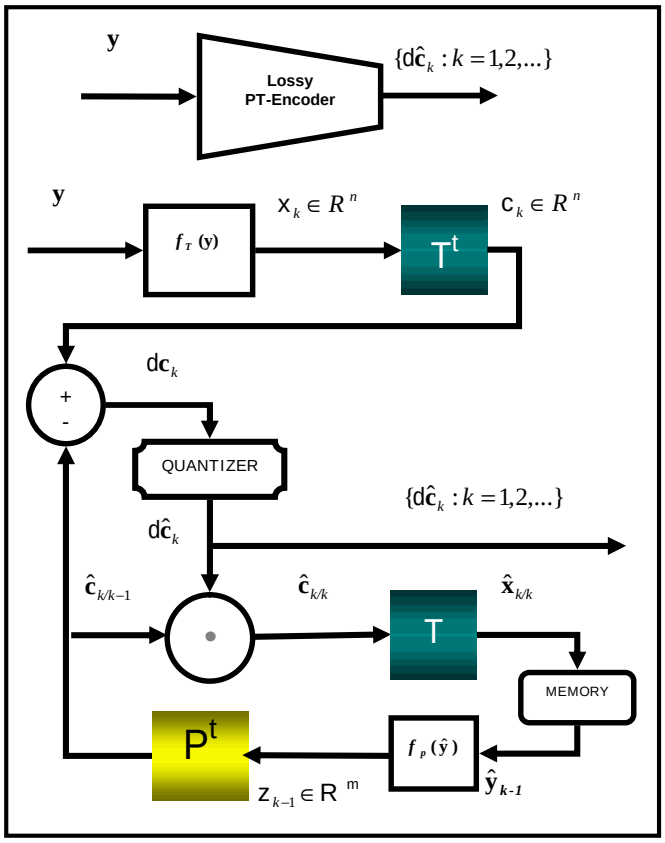

Fig. 2 Lossy PT Encoder Structure

$\mathbf{x}_k$ then becomes the input of an nxn dimensional unitary transform matrix T. The multiplication of the transform matrix T by the pixel vector $\mathbf{x}_k$ produces an n dimensional real valued coefficient column vector $\mathbf{c}_k$. This coefficient, in turn, is predicted by a real n dimensional vector $\hat{\mathbf{c}}_{k/k-1}$. The prediction vector $\hat{\mathbf{c}}_{k/k-1}$ is derived by multiplying the real m dimensional output $\mathbf{z}_{k-1}$ of a predictor pre-processor (constructed using previously encoded pixel vectors as will be seen shortly), by a m x n dimensional real prediction matrix P. A real n dimensional coefficient error $\delta\mathbf{c}_k$ is then formed and subsequently quantized yielding $\delta\hat{\mathbf{c}}_k$. The quantizer has two assumed structures. One is an "analog" structure that is used to derive analytical design expressions for the P and T matrices and another is a "digital" structure used in actual compression applications. The analog structure consists of allowing the most energetic elements of $\delta\mathbf{c}_k$ to pass to the quantizer output unaffected and the remaining elements to appear at the quantizer output as zero values, i.e.,

$$d\hat{\mathbf{c}}_k(i) = \begin{cases} d\mathbf{c}_k(i) & i = 1,...,d \\ 0 & i = d+1,...n \end{cases}. \qquad (2.1)$$

The digital structure consists of multiplying $\delta\mathbf{c}_k$ by a real and scalar compression factor 'g' and then finding the closest integer representation for this real valued product, i.e.,

$$d\hat{\mathbf{c}}_k = \lfloor g\,d\mathbf{c}_k + 1/2 \rfloor. \qquad (2.2)$$

The quantizer output $\delta\hat{\mathbf{c}}_k$ is then added to the prediction coefficient $\hat{\mathbf{c}}_{k/k-1}$ to yield a coefficient estimate $\hat{\mathbf{c}}_{k/k}$. Although other types of digital quantizers exist [3] the quantizer used here (2.2) is the simplest one to implement and yields outstanding results as seen in our simulations [2]. The coefficient estimate $\hat{\mathbf{c}}_{k/k}$ is then multiplied by the transformation matrix T to yield the pixel vector estimate $\hat{\mathbf{x}}_{k/k}$. This estimate is then stored in a memory which contains the last available estimate $\hat{\mathbf{y}}_{k-1}$ of the pixel matrix $\mathbf{y}$. Note that the initial value for $\hat{\mathbf{y}}_{k-1}$, i.e., $\hat{\mathbf{y}}_0$, can be any reasonable estimate for each pixel. For instance, since the processing of the image is done in a sequential manner using prediction from pixel block to pixel block, the initial $\hat{\mathbf{y}}_0$ can be constructed by assuming for each of its pixel estimates

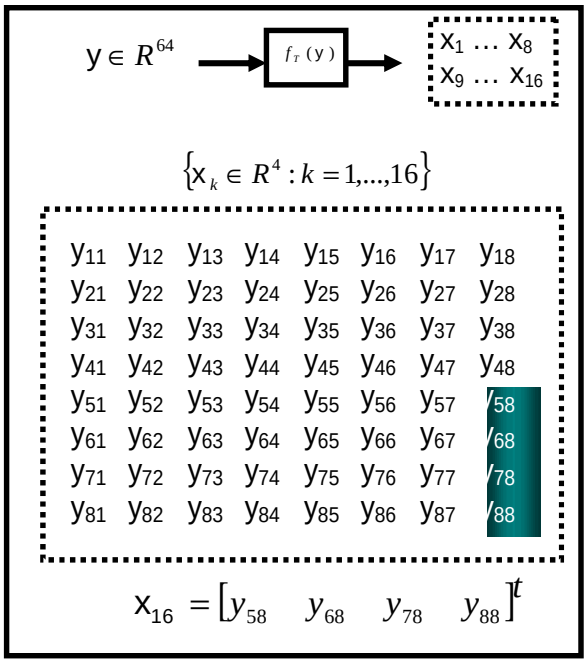

Fig. 3 Image Coding Illustration:Transform Pre-Processing

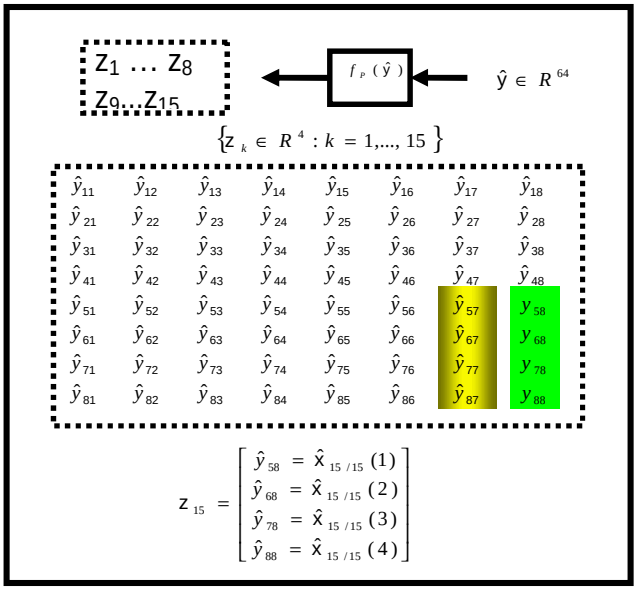

Fig. 4 Image Coding Illustration: Prediction Pre-Processing

the average value of the pixel block $\mathbf{x}_1$. Fig. 4 shows for the illustrative example how the image estimate at processing stage k=16, i.e., $\hat{\mathbf{y}}_{k-1}= \hat{\mathbf{y}}_{15}$, is used by the predictor pre-processor to generate the pixel estimate predictor pre-processor vector $\mathbf{z}_{15}$. Also note from the same figure how at stage k=16 the 4 scalar elements $(\hat{y}_{57}, \hat{y}_{67}, \hat{y}_{77}, \hat{y}_{87})$ of the 8x8 pixel matrix $\hat{\mathbf{y}}_{15}$ are updated making use of the most recently derived pixel vector estimate $\hat{\mathbf{x}}_{15/15}$. Next the design of the T and P matrices of the PT source coder is reviewed.

The design equations for the T and P matrices are derived by minimizing the mean squared error expression

$$E[(\mathrm{x}_k - \hat{\mathrm{x}}_{k/k})^t (\mathrm{x}_k - \hat{\mathrm{x}}_{k/k})] \qquad (2.3)$$

with respect to T and P and subject to three constraints. They are:

1) The elements of $\delta\mathbf{c}_k$ are uncorrelated from each other.
2) The elements of $\delta\mathbf{c}_k$ are zero mean.
3) The analog quantizer of (2.1) is assumed.

After this minimization is performed coupled Wiener-Hopf and Eigensystem design equations are derived [4]. They are:

$$P = [I_m \quad 0_{mx1}]\, J\, T, \qquad (2.4)$$

$$\left\{E[\mathrm{x}_k \mathrm{x}_k^t] - [E[\mathrm{x}_k \mathrm{z}_{k-1}^t] \quad E[\mathrm{x}_k]]\, J\right\} T = T\, \Lambda \qquad (2.5)$$

$$J = \begin{bmatrix} E[\mathrm{z}_{k-1}\mathrm{z}_{k-1}^t] & E[\mathrm{z}_{k-1}] \\ E[\mathrm{z}_{k-1}^t] & 0 \end{bmatrix}^{-1} \begin{bmatrix} E[\mathrm{z}_{k-1}\mathrm{x}_k^t] \\ E[\mathrm{x}_k^t] \end{bmatrix} \qquad (2.6)$$

where these expressions are a function of the first and second order statistics of $\mathbf{x}_k$ and $\mathbf{z}_{k-1}$ including their cross correlation. To find these statistics the following isotropic model for the pixels of $\mathbf{y}$ can be used [4]:

$$E[y_{ij}] = K, \qquad (2.7)$$

$$E[(y_{ij} - K)(y_{i+v,j+h} - K) = (P_{avg} - K^2)\, \mathrm{r}^{D} \qquad (2.8)$$

$$D = \sqrt{(rv)^2 + h^2} \qquad (2.9)$$

$$\mathrm{r} = E[(y_{ij} - K)(y_{i,j+1} - K)]/(P_{avg} - K^2) \qquad (2.10)$$

where v and h are integers, K is the average value of any pixel, P_{avg} is the average power associated with each pixel, and r is a constant that reflects the relative distance between two adjacent vertical and two adjacent horizontal pixels (r =1 when the vertical and horizontal distances are the same).

In Fig. 5 the lossy PT decoder is shown and is noted to be identical in structure to the feedback section of the encoder section of Fig. 2. Next we adapt the aforementioned predictive-transform methodology to the subband memory space compression of images.

III. Subband Predictive –Transform Source Coding

The proposed scheme is next advanced by considering in detail a simple example that integrates the PT source coding

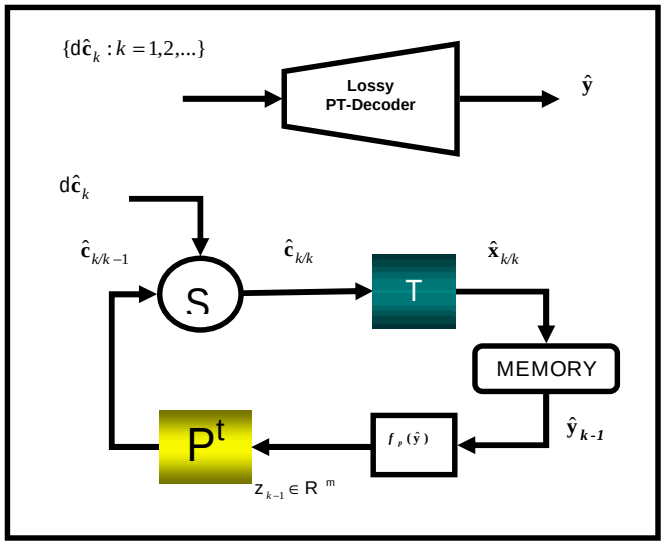

Fig. 5 Lossy PT Decoder

scheme with the wavelets JPEG2000 subband approach. More specifically, we consider the compression of the 4x4 dimensional image depicted in Fig. 6 where $y(i,j)$ denotes a pixel with the order pair (i,j) conveying the spatial location of the pixel.

The subband PT (SPT) algorithm begins with the evaluation of the average value x_0 of the given image {y(i,j)}, i.e.,

$$x_0 = \frac{1}{16} \sum_{i=1}^{4} \sum_{j=1}^{4} y(i, j) \qquad (3.1)$$

This average value can be encoded with 8 bits.

Next the first subband is encoded as shown in Fig. 7. The picture contains three large squares where in each case it is internally made up of four smaller squares. The first large square to discuss is the one located on the lower left hand side of the image. It contains four scalar average

y(1,1)	y(1,2)	y(1,3)	y(1,4)
y(2,1)	y(2,2)	y(2,3)	y(2,4)
y(3,1)	y(3,2)	y(3,3)	y(3,4)
y(4,1)	y(4,2)	y(4,3)	y(4,4)

Fig. 6 The Original 4x4 Image

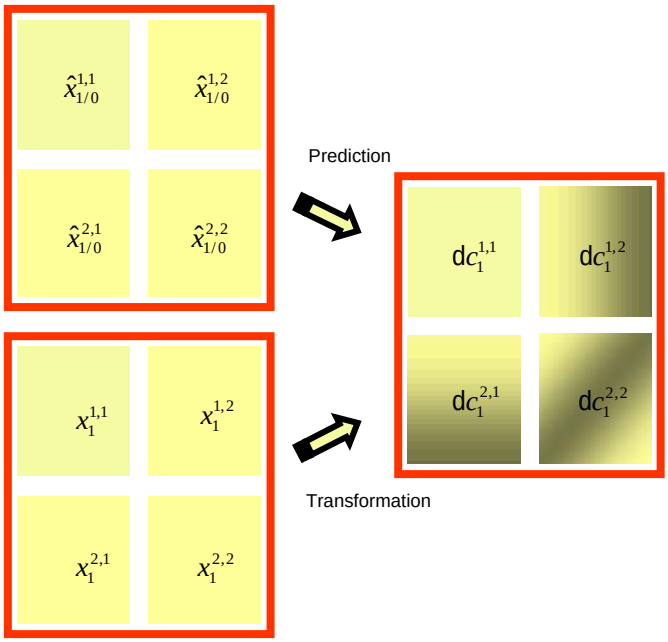

Fig. 7 First Subband Predictive-Transform Pass

values $\{x_1^{k,l} : k = 1,2 \,\&\, l = 1,2\}$ where $x_1^{k,l}$ denotes the average value of four adjacent pixels, i.e.,

$$x_1^{k,l} = \frac{1}{4} \sum_{i=2k-1}^{2k} \sum_{j=2l-1}^{2l} y(i,j) \tag{3.2}$$

These four values are in turn collected into the 4 dimensional column vector $\mathbf{x}_1$, i.e.,

$$\mathbf{x}_1 = [x_1^{1,1} \;\; x_1^{2,1} \;\; x_1^{1,2} \;\; x_1^{2,2}]^t . \tag{3.3}$$

This vector is then multiplied by a 4x4 unitary transform matrix T to generate the coefficient vector c_1, i.e.,

$$\mathbf{c}_1 = T^t \mathbf{x}_1 . \tag{3.4}$$

Clearly, when this transformation matrix is the Hadamard transform we have the standard wavelets JPEG2000 approach [1]. The second large square to investigate is placed on the upper left hand side of the image. It displays the predicted values for the four pixel averages (3.3). These predicted values are denoted by the set of four scalar elements $\{\hat{x}_{1/0}^{k,l} : k = 1,2 \,\&\, l = 1,2\}$ where 'all' of these elements are given the same value of x_0 which is, as mentioned earlier, the average value of the entire image (3.1). It then follows that our prediction vector for the transform coefficients is defined by the expression

$$\mathbf{z}_0 = \begin{bmatrix} \hat{x}_{1/0}^{1,1} \\ \hat{x}_{1/0}^{2,1} \\ \hat{x}_{1/0}^{1,2} \\ \hat{x}_{1/0}^{2,2} \end{bmatrix} = \begin{bmatrix} x_0 \\ x_0 \\ x_0 \\ x_0 \end{bmatrix} \tag{3.5}$$

The prediction vector $\mathbf{z}_0$ is then multiplied by a 4x4 prediction matrix P resulting in the prediction coefficient vector $\hat{\mathbf{c}}_{1/0}$, i.e.,

$$\hat{\mathbf{c}}_{1/0} = P^t \mathbf{z}_0 \tag{3.6}$$

Next the design of T and P is addressed by using the isotropic image correlation model (2.7)-(2.10) with the real constant value of 's' added to $(rv)^2 + h^2$. This is done to reflect the fact that the prediction (3.5) and predicted (3.3) averaged pixels are derived from the same pixel space but are extracted from different subband passes. Furthermore, assigning 0.99999 to both ρ and r, and using any value for K, the following T and P realizations are obtained when s=4:

$$T = \begin{bmatrix} 0.5 & -0.5 & 0.5 & 0.5 \\ 0.5 & -0.5 & -0.5 & -0.5 \\ 0.5 & 0.5 & 0.5 & -0.5 \\ 0.5 & 0.5 & -0.5 & 0.5 \end{bmatrix} \tag{3.7}$$

$$P = \begin{bmatrix} 0.5000 & -0.1545 & 0.1486 & 0.0172 \\ 0.5000 & -0.1545 & -0.1486 & -0.0172 \\ 0.5000 & 0.1545 & 0.1486 & -0.0172 \\ 0.5000 & 0.1545 & -0.1486 & 0.0172 \end{bmatrix} \tag{3.8}$$

Notice that the transform matrix (3.7) is the Hadamard transform [1]. However, this will not be the case in general when using a different averaged pixel block size. The difference between the coefficient vector $\mathbf{c}_1$ and its predicted value $\hat{\mathbf{c}}_{1/0}$ then results in the 4 dimensional coefficient error or innovation $\delta\mathbf{c}_1$, i.e.,

$$\mathrm{d}\mathbf{c}_1 = \begin{bmatrix} \mathrm{d}c_1^{1,1} \\ \mathrm{d}c_1^{2,1} \\ \mathrm{d}c_1^{1,2} \\ \mathrm{d}c_1^{2,2} \end{bmatrix} = \mathbf{c}_1 - \hat{\mathbf{c}}_{1/0} = T^t \mathbf{x}_0 - P^t \mathbf{z}_0 , \tag{3.9}$$

The four elements of $\delta\mathbf{c}_1$ are depicted on the third large square located on the right hand side of Fig. 7. Note that attached to each of these coefficients errors is a background square with its shading representing the 2D drawing of the associated eigenvector that is extracted from the transform matrix (3.7). For instance, the shading associated with the coefficient $\mathrm{d}c_1^{1,1}$ element is uniform in appearance since it corresponds to the DC eigenvector shown on the first column of the Hadamard transform (3.7).

Next, the coefficient error is quantized [1] yielding the quantization coefficient error $\mathrm{d}\hat{\mathbf{c}}_1$, i.e.,

$$\mathrm{d}\hat{\mathbf{c}}_1 = \begin{bmatrix} \mathrm{d}\hat{c}_1^{1,1} \\ \mathrm{d}\hat{c}_1^{2,1} \\ \mathrm{d}\hat{c}_1^{1,2} \\ \mathrm{d}\hat{c}_1^{2,2} \end{bmatrix} = Q(\mathrm{d}\mathbf{c}_1) \tag{3.10}$$

The prediction coefficient vector $\hat{\mathbf{c}}_{1/0}$ is then added to the quantized coefficient error $d\hat{\mathbf{c}}_1$ to yield the estimated coefficient vector $\hat{\mathbf{c}}_{1/1}$, i.e.,

$$\hat{\mathbf{c}}_{1/1} = \hat{\mathbf{c}}_{1/0} + d\hat{\mathbf{c}}_1 . \tag{3.11}$$

The estimated coefficient vector is then multiplied by the Hadamard transform (3.7) to yield an estimate $\hat{\mathbf{x}}_{1/1}$, i.e.,

$$\hat{\mathbf{x}}_{1/1} = \begin{bmatrix} \hat{x}^{1,1}_{1/1} \\ \hat{x}^{2,1}_{1/1} \\ \hat{x}^{1,2}_{1/1} \\ \hat{x}^{2,2}_{1/1} \end{bmatrix} = T\hat{\mathbf{c}}_{1/1} . \tag{3.12}$$

of the 'first' subband average pixel values $\mathbf{x}_1$ (3.3). This completes the first subband pass of the 4x4 pixel image of Fig. 6.

The description of the second and last subband pass of the proposed algorithm begins with an explanation of Fig. 8. As with Fig. 7, this figure is characterized by three large squares. In turn each of these large squares consists of four identical sub-squares where each sub-square in conjunction with the corresponding sub-squares of the other two large squares can be explained similarly as was done earlier for the first subband pass. Furthermore, the required processing associated with each sub-square case will be found later to be perfectly independent of any processing pertaining to the remaining three sub-square cases. Thus parallelism can be used to yield a processing speed for this second subband pass that is governed by that of anyone of the identical

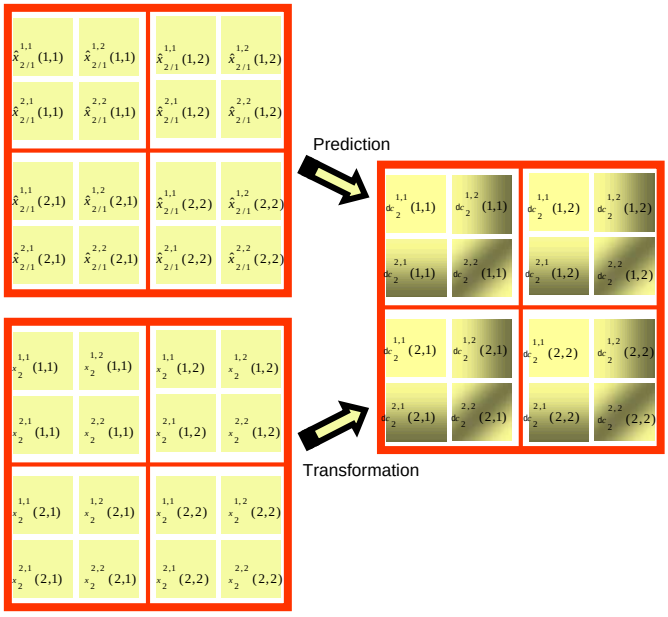

Fig. 8 Second Subband Predictive-Transform Pass

sub-squares. The defining processing expressions for any sub-square case are next discussed in detail.

As was the case for the first subband pass the discussion begins with the large square located on the lower left hand side of the figure. Its four sub-squares, as is also the case for the other two large squares, are differentiated from each other by the order pair set (k,l), i.e.,

$$(k,l) \in \{(1,1),(2,1),(1,2),(2,2)\} , \tag{3.13}$$

as seen from the picture. For each (k,l) sub-square case the following 4 dimensional column vector $\mathbf{x}_2(k,l)$ is then defined

$$\mathbf{x}_2(k,l) = \begin{bmatrix} x_2^{1,1}(k,l) \\ x_2^{1,2}(k,l) \\ x_2^{2,1}(k,l) \\ x_2^{2,2}(k,l) \end{bmatrix} \tag{3.14}$$

where

$$x_2^{i,j}(k,l) = y(i+2(k-1),\, j+2(l-1)), \quad for\ \forall(i,j,k,l) \tag{3.15}$$

This vector is then multiplied by the Hadamard transform matrix T to generate the coefficient vector $c_2(k,l)$, i.e.,

$$\mathbf{c}_2(k,l) = T^t \mathbf{x}_2(k,l) . \tag{3.16}$$

The second large square on the upper left hand side of the image displays the prediction vector

$$\hat{\mathbf{x}}_{2/1}(k,l) = \begin{bmatrix} \hat{x}^{1,1}_{2/1}(k,l) \\ \hat{x}^{1,2}_{2/1}(k,l) \\ \hat{x}^{2,1}_{2/1}(k,l) \\ \hat{x}^{2,2}_{2/1}(k,l) \end{bmatrix} = \begin{bmatrix} \hat{x}^{k,l}_{1/1} \\ \hat{x}^{k,l}_{1/1} \\ \hat{x}^{k,l}_{1/1} \\ \hat{x}^{k,l}_{1/1} \end{bmatrix} \tag{3.17}$$

for the four pixels in (3.14). Note that all the elements in the prediction sub-square (k,l) are predicted with the same identical scalar value $\hat{x}^{k,l}_{1/1}$ that is available from the first subband pass. It now follows that our prediction vector for the transform coefficient vector $\mathbf{c}_2(k,l)$ is defined by the expression

$$\mathbf{z}_1(k,l) = \hat{\mathbf{x}}_{2/1}(k,l) . \tag{3.18}$$

The prediction vector $\mathbf{z}_1(k,l)$ is then multiplied by the 4x4 prediction matrix P resulting in the prediction coefficient vector $\hat{\mathbf{c}}_{2/1}(k,l)$, i.e.,

$$\hat{\mathbf{c}}_{2/1}(k,l) = P^t \mathbf{z}_1(k,l) . \tag{3.19}$$

The difference between the coefficient vector $c_2(k,l)$ and its predicted value $\hat{\mathbf{c}}_{2/1}(k,l)$ then results in the 4 dimensional coefficient error or innovation $dc_2(k,l)$, i.e.,

$$\mathrm{d}\mathbf{c}_2(k,l)=\begin{bmatrix}\mathrm{d}c_2^{1,1}(k,l)\\ \mathrm{d}c_2^{2,1}(k,l)\\ \mathrm{d}c_2^{1,2}(k,l)\\ \mathrm{d}c_2^{2,2}(k,l)\end{bmatrix}=\mathbf{c}_2(k,l)-\hat{\mathbf{c}}_{2/1}(k,l) \quad (3.20)$$

that is plotted in the third large square of Fig. 8. This coefficient error is then quantized to yield the quantized coefficient error

$$\mathrm{d}\hat{\mathbf{c}}_2(k,l)=Q(\mathrm{d}\mathbf{c}_2(k,l)). \quad (3.21)$$

A coefficient estimate $\hat{\mathbf{c}}_{2/2}(k,l)$ of the coefficient vector $\mathbf{c}_2(k,l)$ is then obtained by adding the predicted coefficient vector to the quantized coefficient error to yield

$$\hat{\mathbf{c}}_{2/2}(k,l)=\hat{\mathbf{c}}_{2/1}(k,l)+\mathrm{d}\hat{\mathbf{c}}_2(k,l) \quad (3.22)$$

Finally an estimate of the pixels (3.14)-(3.15) $\hat{\mathbf{x}}_{2/2}(k,l)$ is derived by multiplying the coefficient estimate (3.22) by the Hadamard transform to yield

$$\hat{\mathbf{x}}_{2/2}(k,l)=T\hat{\mathbf{c}}_{2/2}(k,l). \quad (3.23)$$

This concludes the subband PT source coding methodology that can be readily extended to arbitrary size images.

In Fig. 9 the quantized 'coefficient errors' are displayed using the standard subband display [1]. Clearly, when the aforementioned prediction mechanism presented in (3.9) and (3.20) is inhibited the classical wavelets structure is derived which consists of quantized 'coefficients' as shown in Fig. 10.

Next in Figs. 12 the result is shown when the Lena image of Fig. 11 is highly compressed. Seven subbands were used where the prediction of each 2x2 pixel block was performed using 'nine' 2x2 constant pixel block estimates derived from the previously encoded subband as seen from Fig. 13. The corresponding transform matrix T for this scheme was once again the Hadamard transform of (3.7) and for the prediction matrix P the following 36x4 matrix was derived

P =

0.0257	-0.0070	0.0076	-0.0027
0.0170	-0.0093	0.0050	-0.0039
0.0273	-0.0158	0.0041	-0.0032
0.0273	-0.0158	-0.0033	0.0024
0.0170	-0.0093	-0.0046	0.0034
0.0257	-0.0070	-0.0069	0.0019
0.0170	-0.0047	0.0097	-0.0039
0.0335	-0.0210	0.0217	-0.0152
0.0802	-0.0508	0.0222	-0.0165
0.0802	-0.0508	-0.0199	0.0139
0.0335	-0.0210	-0.0208	0.0141
0.0170	-0.0047	-0.0092	0.0034
0.0274	-0.0034	0.0165	-0.0033
0.0803	-0.0204	0.0527	-0.0165
0.1917	-0.0541	0.0585	-0.0225
0.1917	-0.0541	-0.0532	0.0163
0.0803	-0.0204	-0.0505	0.0140
0.0274	-0.0034	-0.0158	0.0024
0.0274	0.0034	0.0158	0.0024
0.0803	0.0204	0.0505	0.0140
0.1917	0.0541	0.0532	0.0163

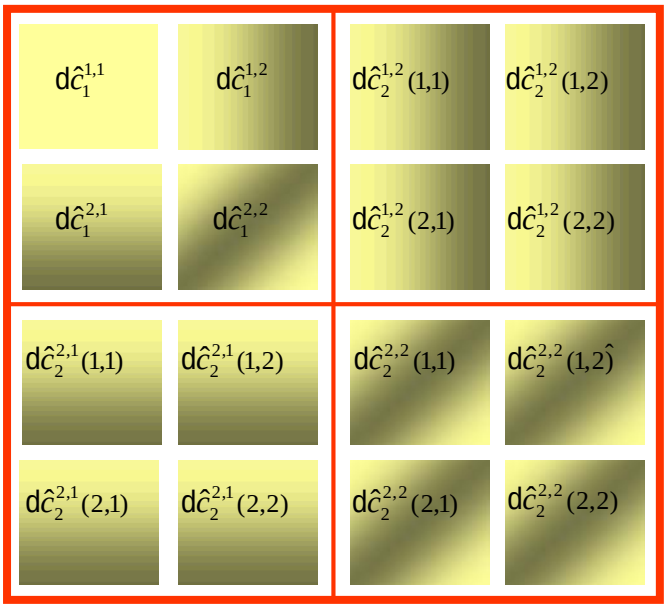

Fig. 9 Coefficient Error Arrangement Using Standard Subband Organization

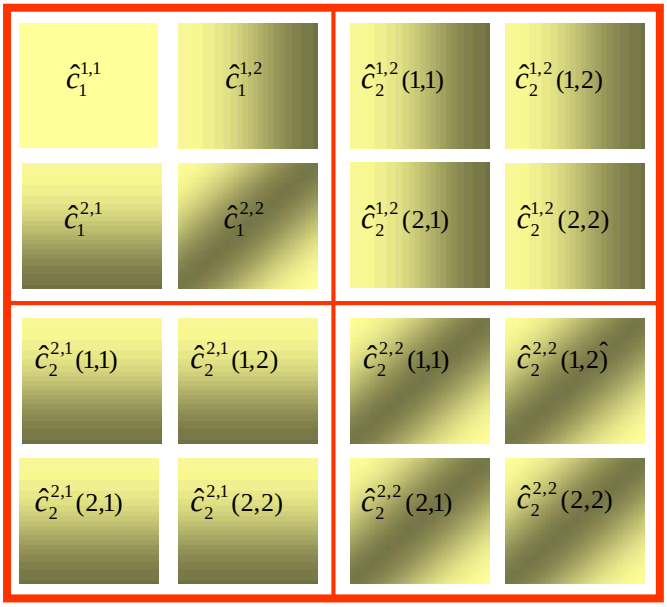

Fig. 10 Coefficient Arrangement Using Standard Subband Organization

0.1917	0.0541	-0.0585	-0.0225
0.0803	0.0204	-0.0527	-0.0165
0.0274	0.0034	-0.0165	-0.0033
0.0170	0.0047	0.0092	0.0034
0.0335	0.0210	0.0208	0.0141
0.0802	0.0508	0.0199	0.0139
0.0802	0.0508	-0.0222	-0.0165
0.0335	0.0210	-0.0217	-0.0152
0.0170	0.0047	-0.0097	-0.0039
0.0257	0.0070	0.0069	0.0019
0.0170	0.0093	0.0046	0.0034
0.0273	0.0158	0.0033	0.0024
0.0273	0.0158	-0.0041	-0.0032
0.0170	0.0093	-0.0050	-0.0039
0.0257	0.0070	-0.0076	-0.0027

Fig. 11 The original Lena image

Fig. 12 MMSE PT compressed Lena image

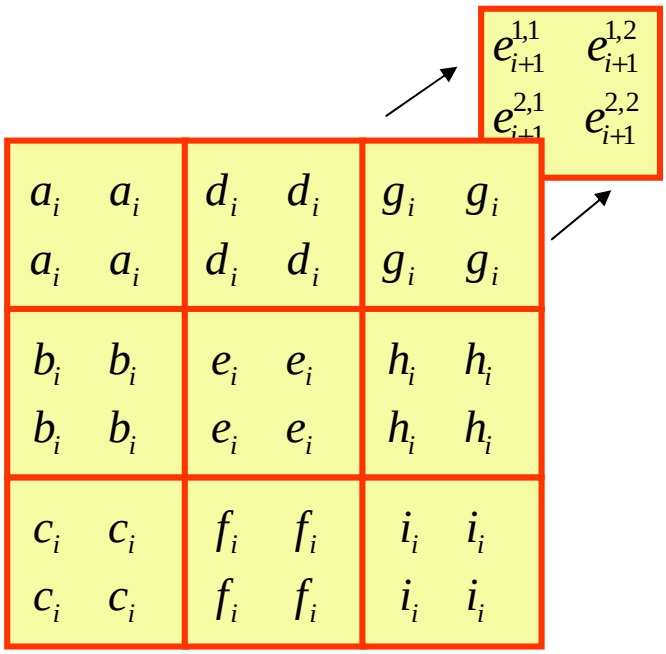

Fig. 13 Prediction geometry from nine 2x2 constant pixel block estimates in i^{th} subband to 2x2 pixel block in $(i+1)^{th}$ subband

The PSNR of the MMSE PT compressed Lena image of Fig. 12 is 29.51 dBs and the number of bytes needed for its storage is 3,395 bytes which in JPEG2000 produces a compressed Lena image with PSNR of 28.84 dBs. The aforementioned number of bytes was achieved using a subband version of the straightforward bit planes methodology introduced in [2]. Nonlinear quantizers were applied to the last subband coefficient errors where gaussian distributions were assumed for them. In addition, the linear quantizer of (2.2) with g = 0.025 was used for the remaining subbands. Notice the acceptable visual image quality derived for such a high level of compression. Clearly a better perceptual image quality as well as a greater compression level may be achieved with the use of nonlinear quantizers for all subbands and/or some appropriate type of post-processing.

The best image isotropic model parameter 's' value to use for each possible level of compression and/or subband remains to be investigated. In addition, it is noticed that the proposed methodology can be readily applied to any averaged pixel block size processing structure which naturally includes that of a strip processor [2]. This problem is being investigated and further results will be forthcoming in the near future.

References

[1] Taubman, D. S. and Marcellin, M., *JPEG2000: Image Compression Fundamentals, Standards and Practice*, Kluwer Academic Publishers, MA, 2002

[2] Feria, E. H. and Licul, D., "A Bit Planes Predictive-Transform Source Coder Illustrated with SAR Imagery", *Proceedings of SPIE Defense and Security Symposium*, 17-21 April 2006

[3] Yeung, R. W., A First Course in Information Theory, Kluwer Academic Publishers, New York, 2002

[4] Feria, E.H., "Decomposed Predictive-Transform Estimation", IEEE Transactions on Signal Processing, Vol. 42, No. 10, pp. 2811-2822, October 1994

[5] Guerci, J.R. and Baranoski, E.J., "Knowledge-Aided Adaptive Radar at DARPA", *IEEE Signal Processing Magazine*, vol. 23, no. 1, pp. 41-50, January 2006

[6] Feria, E.H. and Agaian, S. A, "Accelerated Predictive-Transform", *Proceedings of IEEE ICASSP*, May 2002